Heliyon 8 (2022) e11988

Contents lists available at ScienceDirect

Heliyon

journal homepage: www.cell.com/heliyon

Research article

Modeling of the stability of water-based graphite dispersions using polyvinylpyrrolidone on the basis of the DLVO theory

Cara Greta Kolb *, Maja Lehmann, Dominik Kulmer, Michael Friedrich Zaeh

Institute for Machine Tools and Industrial Management, Technical University of Munich, Germany

ARTICLE INFO

Keywords:
Nanoparticle dispersions
Graphite dispersions
Stability
DLVO
Zeta potential
Polyvinylpyrrolidone

ABSTRACT

The applications of graphite nanoparticle dispersions emerge due to the increasing importance of printed electronics and microelectronics, lithium-ion batteries, and supercapacitors. Promising technologies are inkjet printing processes, which are significantly influenced by the dispersion stability. Achieving stability is particularly challenging for nanoparticle dispersions due to the strong attractive forces emanating from the large particle surfaces. Despite the significance attributed to stability, it is predominantly investigated empirically. The only existing model to mathematically describe interparticle forces is given by the DLVO theory. This paper uses the extended DLVO theory to model the stability of aqueous graphite dispersions. Furthermore, the influences arising from an electrosterically stabilizing dispersant, in this case polyvinylpyrrolidone (PVP), were incorporated in the model. Experimentally data obtained from sedimentation analyses concur with the DLVO theory prediction. Due to the universality of the model, it is expected to be applicable to different material and dispersant systems.

1. Introduction

The ever-increasing demand for small-scale functionalized products has driven the development of printable nanoparticle dispersions [1]. In particular, with the increasing interest in portable and wearable devices, the applications of carbon nanoparticle dispersions are burgeoning [2, 3]. Dispersions based on graphite and graphene currently dominate this field due to the inherent high electrical conductivity and electrochemical potential, respectively. Graphite represents the predominant anode active material in lithium-ion batteries [4]. Currently, design-optimized battery concepts are explored, allowing for performance-optimized batteries with potentials for customization and flexibility [5]. The applications of graphene range from electronics and microelectronics incorporating additional smart functions [2] to efficient energy storage devices, such as supercapacitors [6, 7]. Processes that enable selective material dispensing are predestined for the fabrication of these products. However, these technologies place special demands on the dispersions [8]. This applies in particular to drop-on-demand inkjet printing processes [9], in which a high-resolution structure is formed by the dropwise deposition and the coalescence of a dispersion on a substrate [10, 11]. The dispersions are required to show a high stability over time, which prevents the particles from coagulation and consequently sedimentation [12]. Instable dispersions negatively affect the drop formation and the risk of nozzle clogging is increased [13, 14]. Due to the strong attractive forces caused by the large particle surface, aqueous graphite [15] and graphene [16] nanoparticle dispersions are very prone to coagulation. Therefore, dispersants are needed to stabilize the particles in the medium [17]. In previous empirical studies [18, 19], we have demonstrated that the use of the electrosterically stabilizing dispersant polyvinylpyrrolidone (PVP) effectively counteracts the strong attractive interactions between the graphite particles, leading to a homogeneous distribution of the particles in the dispersion. The particle size distribution of the primary particles with an initial diameter in the lower nanometer range was found to be below the threshold for printing [20] when the suitable particle-dependent dispersant content is added. Htwe and Mariatti [21] reported that PVP is also able to efficiently disperse and stabilize graphene particles in water. The prepared inks were processed via inkjet printing processes, although the particle size distribution achieved by PVP was not specified.

Despite the relevance attributed to the dispersion stability in terms of printability, the effectiveness of dispersants is predominantly investigated empirically through extensive studies. There are hardly any theoretical approaches to describe the complex physical phenomena

* Corresponding author.
E-mail addresses: cara.kolb@iwb.tum.de (C.G. Kolb), maja.lehmann@iwb.tum.de (M. Lehmann).

https://doi.org/10.1016/j.heliyon.2022.e11988
Received 20 October 2022; Received in revised form 7 November 2022; Accepted 23 November 2022

driven by the kinetic and thermal interactions that underlie the nature of nanoparticle dispersions.

To the knowledge of the authors, the only established approach to mathematically describe the energetic interactions in nanoparticle dispersions and thus the stability behavior is given by the DLVO theory [22]. It was independently developed in the 1940s by Derjaguin and Landau [23] and Verwey and Overbeek [24].

This theory explains the effect of particle interactions in dispersions by determining the potential energy between the particles. The total interaction energy V_T is a result of the entirety of repulsive and attractive interactions as a function of the particle distance h. According to the theory in its original form, two major forces act on the particles in a dispersion, in particular the repulsive electrostatic forces induced by the electrochemical double layers and the attractive van-der-Waals-London forces. However, various studies have shown that the consideration of the forces postulated in the original DLVO theory alone is not sufficient to obtain a well-founded statement about the stability of all types of dispersions [25, 15]. Accordingly, extensions of the DLVO theory have been elaborated over the years. The state-of-the-art extended DLVO theory also takes into account the depletion forces, the steric forces, and the hydrophobic forces, which are summarized under the term non-DVLO forces [26].

In the following, the studies on the DLVO theory are summarized in the context of graphite dispersions and for other applications.

DLVO theory in the context of graphite and graphene dispersions

Liu et al. [27] conducted empirical studies on graphite dispersions. These ranged from investigations of the zeta potential as a function of the pH value to wettability and aggregation. Based on their analysis, they concluded that the classical DLVO theory is sufficient to describe graphite dispersions due to the low degree of hydration.

In contrast, Yangshuai et al. [15] argued that the stability behavior of graphite dispersions can be fully described by applying only the extended DLVO theory. In the extended model presented, the van-der-Waals-London forces, the electrostatic forces, and the hydrophobic forces were taken into account. On this basis, the results of the extended theory were compared with those of the DLVO theory in its original form.

Wakamatsu and Numata [28] investigated the reuse of graphite from the steel and iron industries, where graphite is produced in large quantities as a byproduct of fly ash. To further separate impurities, graphite is recovered by flotation. This process utilizes the selective binding of fine particles to air bubbles versus the binding to other particles. The empirical studies demonstrate the pH value dependence of the zeta potential on the associated degree of flotation. The DLVO theory is not explicitly addressed, but is indirectly considered through the zeta potential.

Gudarzi [29] presented a model based on the classical DLVO theory that captures the stability of graphene oxide (GO) and reduced graphene oxide (rGO). The predictability of the model was evaluated by determining the critical coagulation concentration in monovalent salt solutions. This parameter is defined as the threshold electrolyte concentration, above which the particles agglomerate rapidly due to the compressed double layer. Experiments revealed that the experimentally determined CCC corresponds to the values obtained from the model.

Further applications of the DLVO theory

Mitchell et al. [25] demonstrated a well-founded model of the extended DLVO theory to describe the phenomena that occur during the flotation of copper and iron minerals for separation. They considered the van-der-Waals-London forces, the electrostatic forces, and the hydrophobic forces. The absolute value of the zeta potential and the dependence on the pH value were measured. The interaction curves were then calculated from the potentials. Subsequent flotation experiments demonstrated the accuracy of the calculations by allowing the selective flotation of the individual minerals in the calculated pH value range.

Yoon et al. [30] investigated the interaction between the bubbles and the particles during flotation, with a focus on the hydrophobic interactions. They developed a model to determine the force constant for the calculation of the hydrophobic forces between the bubbles and the particles in the medium. Accordingly, they calibrated the model to determine the hydrophobic forces and used the extended DLVO theory to calculate the total interaction energies.

Zhu et al. [31] created a 3D simulation model to evaluate the coagulation of carbon black and cathode active materials in an N-Methyl-2-pyrrolidone (NMP) medium containing polyvinylidene fluoride (PVDF) on the basis of Brownian motion. They used the van-der-Waals-London forces and the electrostatic forces to calculate the interaction of the particles as a function of the separation distance. The empirical validation showed that the model describes quite well the coagulation behavior as a function of the temperature and the mass fraction of the respective components.

It follows from the consideration of the state of the art that the majority of models based on the DLVO theory have been developed to describe flotation phenomena. In particular, there are hardly any approaches available to model the stability of graphite and graphene dispersions. To the knowledge of the authors, the influence of dispersants on the particle-particle interactions has not yet been investigated, although previous studies showed that their use is indispensable to achieve dispersion stability.

Approach

In this paper, an analytical model on the basis of the extended DLVO theory is elaborated to describe the stability of aqueous graphite dispersions containing the dispersant PVP. Two different PVP derivatives, namely K-17 and K-30, were used for the empirical studies. The total interaction energies are calculated using empirical data obtained from zeta potential measurements and material-specific parameters from the literature. The model is then compared with sedimentation analyses.

2. Modeling on the basis of the extended DLVO theory

The classical DLVO theory takes into account only the repulsion effects due to the electrostatic double layer V_{el} and the attraction caused by the van-der-Waals-London forces V_{vdw}, resulting in the expression for the energy V_T as follows:

$$V_T = V_{el} + V_{vdw}. \tag{1}$$

In addition to the energy fractions incorporated in Equation (1), the extended DLVO theory also accounts for hydrophobic and steric effects as well as depletion. The summation of the energy fractions gives a good approximation of the total energy $V_{T,ex}$, assuming that they are independent of each other [26, 32]. Accordingly, the total interaction energy can be derived as follows:

$$V_{T,ex} = V_{el} + V_{vdw} + V_{hyd} + V_s + V_{dep}. \tag{2}$$

Commonly, the respective interaction energy curves are plotted over the particle distance [33, 34], as schematically depicted in Fig. 1.

In the following, the formulations describing the respective energy fractions are outlined and related to the conditions that apply to graphite dispersions. In addition, the dispersant PVP and the associated effects are included in the model.

Electrostatic double layer interaction

The energy resulting from the electrostatic double layer interaction V_{el} can be described by the Poisson-Boltzmann equation. This model aims to determine the distribution of the electrostatic potential in an ionic solution in the direction perpendicular to the charged particle surface. The model accuracy was reported to be down to particle distances of a few nanometers [35]. In the original version of the DLVO theory, a constant

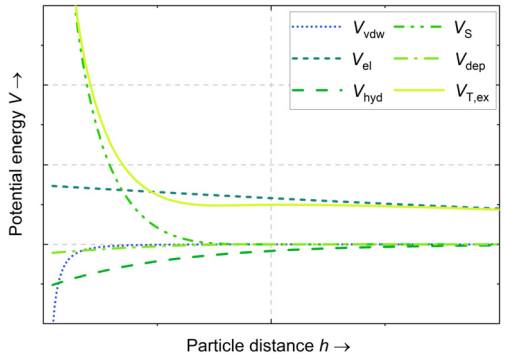

Fig. 1. Schematic depiction of the energy fractions of the extended DLVO theory as a function of the particle distance h; the total interaction energy $V_{T,ex}$ results from the summation of the electrostatic double layer interaction V_{el}, the van-der-Waals-London interaction V_{vdw}, the hydrophobic interaction V_{hyd}, the steric interaction V_s, and the depletion V_{dep} (principle modified from Kumar et al. [33] and Zhang and Zeng [34]).

potential is assumed [24, 23]. This assumption was proven to be valid for surface potentials up to 50 mV [26]. Our previous studies have shown that this applies for the dispersions which are also considered in this paper [18].
With this approximation, V_{el} obeys the following equation:

$$V_{el} = \frac{\pi\epsilon\epsilon_0 a_1 a_2}{a_1 + a_2}[4\psi_1\psi_2 atanh(e^{-\kappa h}) + (\psi_1^2 + \psi_2^2)\ln(1 - e^{-2\kappa h})]. \quad (3)$$

Here, the indices 1 und 2 are used to describe the interaction of two different particles 1 and 2 [26]. a is the radius of the respective particle, ψ the surface potential of the particle, ϵ the dielectric constant of the particle, ϵ_0 the dielectric constant of the medium, h the particle separation distance, and κ the Debye constant. The latter describes the thickness of the electrostatic double layer and is defined as

$$\kappa = \left\{ \frac{e^2 \sum_{i=1}^{\infty} n_i z_i^2}{\epsilon\epsilon_0 k_B T} \right\}^{\frac{1}{2}}, \quad (4)$$

where n_i represents the ionic strength of the type i in the dispersion with the valence z_i. For water at a temperature of 298.15 K (25 °C), a simplified formulaic relationship of Equation (4) applies. The Debye constant can be determined as a function of the ionic strength I, leading to Equation (5) [26]:

$$\kappa = 3.288\sqrt{I} \quad (5)$$

Here, κ is measured in nm^{-1} and I in mol/L [26].

van-der-Waals-London interaction

The model used to describe the van-der-Waals-London interaction energy V_{vdw} is based on the theories of Hamaker [36]. Accordingly, the energy V_{vdw} of two spherical particles with the radii a_1 and a_2 is given as [37]

$$V_{vdw} = -\frac{A_{132}}{6}\left\{ \frac{2a_1a_2}{r^2 - (a_1 + a_2)^2} + \frac{2a_1a_2}{r^2 - (a_1 - a_2)^2} + ln\frac{r^2 - (a_1 + a_2)^2}{r^2 - (a_1 - a_2)^2} \right\}, \quad (6)$$

where r stands for the inter-center separation distance of the two spheres and A_{132} for the Hamaker constant of the dispersion [26].
The Hamaker constant of the dispersion A_{132} (see Equation (6)) can be calculated by combining the constants of the individual particles and the medium [26]. The total expression for A_{132} follows Equation (7):

$$A_{132} = A_{12} + A_3 - A_{13} - A_{23} = \left(\sqrt{A_1} - \sqrt{A_3}\right)\left(\sqrt{A_2} - \sqrt{A_3}\right). \quad (7)$$

Here, the indices 1 and 2 represent the particles and the index 3 the continuous phase. Double indices stand for the combination of the Hamaker constant of mixtures [26].
To account for the electromagnetic retardation on the van-der-Waals-London forces, the effective Hamaker constant is introduced [38, 39]. In this context, Pailthorpe and Russel [40] demonstrated that the use of the effective Hamaker constant yields approximately the same result as the calculation based on the Lifshitz's continuum theory. Nguyen and Schulze [26] formulated a simple approximation of the effective Hamaker constant, where it is divided into a zero frequency part A_{132}^0 (see Equation (8)) and a non-zero frequency part A_{132}^ζ (see Equation (9)).
According to van Guyen et al. [41], for most minerals the zero-frequency part A_{132}^0 can be approximated as follows:

$$A_{132}^0 \approx \frac{3k_BT}{4}. \quad (8)$$

The non-zero frequency part A_{132}^ζ can be expressed as

$$A_{132}^\zeta = \frac{3\hbar\omega}{8\sqrt{2}} \times \frac{(B_1 - B_3)(B_2 - B_3)}{(B_1 + B_3)\sqrt{B_2 + B_3} + (B_2 + B_3)\sqrt{B_1 + B_3}}, \quad (9)$$

where $\hbar$ stands for the Planck's constant divided by 2π, ω for the characteristic relaxation frequency of the ultraviolet spectrum, and B_i for a parameter of the oscillator model. B_i can be approximated by the square of the refractive index of the materials. ω is of the order of magnitude $2 \cdot 10^{16}$ rad/s for most materials [26, 42]. In case of symmetry of the particles, Equation (9) reduces to Equation (10):

$$A_{132}^\zeta = \frac{3\hbar\omega}{16\sqrt{2}}\frac{(B_1 - B_3)^2}{(B_1 + B_3)^{\frac{3}{2}}}. \quad (10)$$

With respect to the electromagnetic retardation effect, the adjusted non-zero frequency term results in Equation (11) with the partial terms Equation (12) and Equation (13):

$$A_{132}^\zeta = \frac{3\hbar\omega}{8\sqrt{2}}\frac{(B_1 - B_3)(B_2 - B_3)}{(B_1 - B_2)} \times \left\{ \frac{I_2}{\sqrt{B_2 + B_3}} - \frac{I_1}{\sqrt{B_1 + B_3}} \right\}, \quad (11)$$

with

$$I_i = 1/[1 + (h/\lambda_i)^q]^{1/q}, \quad (12)$$

and

$$\lambda_i = \frac{c}{\pi^2\omega}\sqrt{\frac{2}{B_3(B_i + B_3)}}. \quad (13)$$

Here, h is the particle separation distance and c the speed of light. q represents a best fit parameter, resulting from a data fitting of the Hamaker-based approximation to the exact solution given by Lifshitz [26].
For symmetric systems, Equation (11) can be reduced, leading to Equation (14):

$$A_{132}^\zeta = \frac{3\hbar\omega}{16\sqrt{2}}\frac{(B_1 + B_3)^2}{(B_1 + B_2)^{3/2}}\left\{1 + \left(\frac{h}{\lambda}\right)^q\right\}^{-\frac{1}{q}}. \quad (14)$$

Taking into account the impact of the electrolyte, the total Hamaker constant A_{132} follows Equation (15):

$$A_{132} = A_{132}^0(1 + 2\kappa h)e^{-2\kappa h} + A_{132}^\zeta. \quad (15)$$

Hydrophobic interaction

Various approaches exist to describe the hydrophobic interaction energy V_{hyd}. An established model is the one given by Yangshuai et al. [15], according to which V_{hyd} is defined as

$$V_{hyd} = -2.51 \cdot 10^{-3} ak\lambda e^{\left(-\frac{h}{\lambda}\right)}, \tag{16}$$

where k is a hydrophobic modification coefficient of 0.4167, a the radius of the particle, and λ the decay length with a value of 5.29 nm [15]. For interactions of different particles, a is replaced by the harmonic mean of the particle radii [25, 26].

Steric interaction

Due to the complex phenomena underlying the interaction of the polymer and the particles, modeling the steric repulsion V_s is not trivial. The following differentiation applies according to Likos et al. [43]:

$$V_s = \begin{cases} \infty, & h < 0 \\ func(h), & 0 < h \leq 2L \\ 0, & 2L < h \end{cases}$$

Here, L stands for the thickness of the layer formed by the polymer chains.

For $h = 0$, the particle surfaces are in direct contact. Accordingly, V_s is not defined for $h < 0$. When h exceeds $2L$, the PVP shells are no longer in contact and no steric repulsion comes into effect.

A possible approach for $func(h)$ is provided by Nguyen and Schulze [26], which leads to the following expression:

$$func(h) = \frac{64L^2 k_B T f}{s^3} \times \left[\frac{1}{5}\left(\frac{h}{2L}\right)^{-\frac{1}{4}} - \frac{1}{77}\left(\frac{h}{2L}\right)^{\frac{11}{4}} + \frac{3}{35}\frac{h}{2L} - \frac{3}{11}\right], \tag{17}$$

with

$$f = \frac{2\pi a_1 a_2}{a_1 + a_2}. \tag{18}$$

Here, f stands for the geometric conversion factor of the Derjaguin approximation and s for the mean distance between the chain attachment points at the surface [26]. In the case of two equal spheres with the radii $a = a_1 = a_2$, Equation (18) simplifies to $f = \pi a$ [42].

From the viscosity measurements of the PVP derivatives K-17 and K-30 (see Fig. 2) it is evident that the molecules fully adsorb at the graphite surface up to a content of 30 m% and 20 m%, respectively. Here, the viscosity values were determined according to the measuring principle described in Kolb et al. [18]. The measurement data are provided in the supplementary files. With the total molecular weight M of the respective PVP derivative, the average number of adsorbed PVP chains N_{ads} can be determined as follows [43, 44]:

$$N_{ads} = \frac{M_{ads}}{M} \cdot N_A. \tag{19}$$

In Equation (19), M_{ads} is the adsorbed mass of the PVP and N_A the Avogradro constant.

The mean attachment distance s (see Equation (17)) can be calculated from the specific surface area A of the graphite used, resulting in Equation (20) (see Table 1) [43, 44]:

$$s = \sqrt{\frac{A}{N_{ads}}}. \tag{20}$$

The expansion of the PVP molecular chains in the solvent depends both on the coverage of the particle surface and the suitability of the solvent for the polymer. Depending on the conditions, the PVP molecular chain can be present as a *globule* (poor conditions), *random coil* (medium conditions) or *expanded coil* (good conditions) (see Fig. 3) [42].

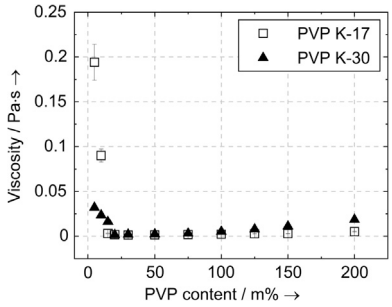

Fig. 2. Viscosity as a function of the PVP content for the PVP derivatives K-17 and K-30.

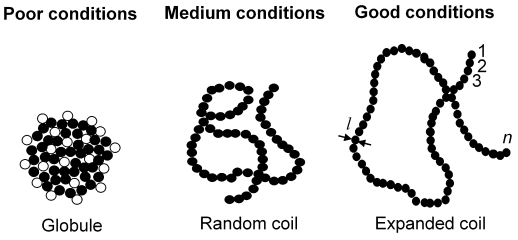

Fig. 3. Different states of a polymer chain in a medium depending on the conditions; each polymer chain consists of n monomer units of the length l (modified from Israelachvili [42]).

Table 1. Properties of the used PVP derivatives.

Symbol	Value	Unit	Reference
M	$M_{K-17} = 10000$ $M_{K-30} = 50000$	g/mol	[46]
M_0	111	g/mol	[47]
A	195	m^2/g	[48]
l	0.154	nm	[47]

The coverage of the surface is expressed by the radius of gyration R_g, which represents a length scale for an unperturbed coil in an ideal solvent. It is defined as [42]

$$R_g = \frac{l \cdot \sqrt{n}}{\sqrt{6}}, \tag{21}$$

where l is the length of a PVP monomer segment and n the number of segments of the PVP molecular chain. n indicates the relation between the total molar mass M and the molar mass of a monomer segment M_0, leading to Equation (22):

$$n = \frac{M}{M_0}. \tag{22}$$

For real, non-ideal solvents, the coil size may deviate from R_g (see Equation (21)), which is expressed by the Flory radius $R_F = \alpha \cdot R_g$ [42]. While for polymers in an unsuitable solvent, α is less than 1, R_F for suitable solvents can be calculated as follows [42]:

$$R_F \approx l \cdot n^{\frac{3}{5}}. \tag{23}$$

Due to the good solubility of the investigated PVP derivatives in water [45], Equation (23) is assumed to be valid for the examined polymer-medium combinations. In this study, for both the derivatives K-17 and K-30, $s > R_g$ applies, which corresponds to a low coverage. When the coverage of the polymer on the particle surface is low and a non-ideal solvent is used, the PVP molecules are present in the medium as *expanded coils*. The thickness of a coil L is approximated by Equation (24):

$$L = 2 \cdot R_F. \tag{24}$$

Depletion

Depletion is caused by dissolved, non-adsorbing polymer molecules that

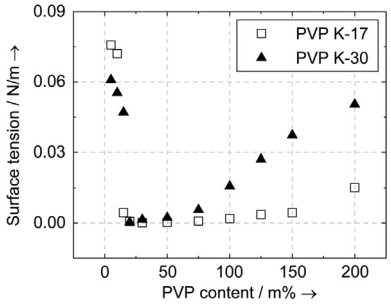

Fig. 4. Surface tension of the graphite dispersions as a function of the PVP content (calculated on the basis of Kolb et al. [18]).

restrict the movement of the particles [49]. However, this diffusion inhibition comes into effect only at higher polymer concentrations. At low polymer concentrations, shells, also known as depletion zones, form around the particles, which promote the formation of agglomerates.
There are several established models to describe the depletion effect V_{dep}. A common approach is the one given by Vincent and Jones [50, 51], leading to the following expression for V_{dep}:

$$V_{dep} = 2 \cdot \pi a \left(\frac{\mu_1 - \mu_1^0}{v_1} \right) \left(\Delta + \delta - q + p - \frac{h}{2} \right)^2 . \quad (25)$$

Here, Δ represents the range of the depletion effect, δ the thickness of the polymer shell, q the compression of the polymer shell, p the extent of the overlap of the polymer shells, and $(\mu_1 - \mu_1^0)/v_1$ the osmotic pressure. Depletion in the context of this paper means that the PVP molecules avoid being absorbed at the graphite surface and prefer the free volume. In this case, the surface tension increases with a rising PVP content [49]. Pelofsky [52] empirically determined a formulaic relationship between the surface tension γ and the viscosity η of a medium, which obeys the following expression:

$$\ln \gamma = \frac{B}{\eta} + \ln A. \quad (26)$$

Here, A and B are dimensional constants of the specific substrate. A represents the intercept and B the slope of the curve. Applying Equation (26) for water, A determines to be 79.10 and B -0.08366 [52].
Taking into account the course of the viscosity of the graphite dispersions as a function of the PVP content presented by Kolb et al. [18], a slight increase in the surface tension is apparent from 30 m% PVP towards higher PVP contents (see Fig. 4). This indicates that up to a PVP content of 30 m% depletion effects can be disregarded.

Superposition of stabilization mechanisms

From the results of the derivations it follows that effects due to depletion (see Equation (25)) can be ignored for the given application. Therefore, Equation (2) with the partial terms Equation (3), Equation (6), Equation (16) and Equation (17) simplifies to:

$$V_{T,ex} = V_{el} + V_{vdw} + V_{hyd} + V_s. \quad (27)$$

3. Materials and methods

3.1. Synthesis of the dispersions

Water-based graphite dispersions with a constant graphite content of 10 m% and a varying PVP content were prepared. For this purpose, high-purity graphite powder (Nanografi, Turkey) suitable for the production of lithium-ion batteries with a mean diameter of 30 nm was employed and PVP was added as a dispersant. Therefore, the PVP derivatives PVP-17 (Luvitec, BASF, Germany) and PVP-30 (Merck, Darmstadt, Germany) were used. The electrolyte employed was NaCl (Carl ROTH, Germany) of laboratory quality (p.a., ACS, ISO) with a purity of ≥ 99.5 %.

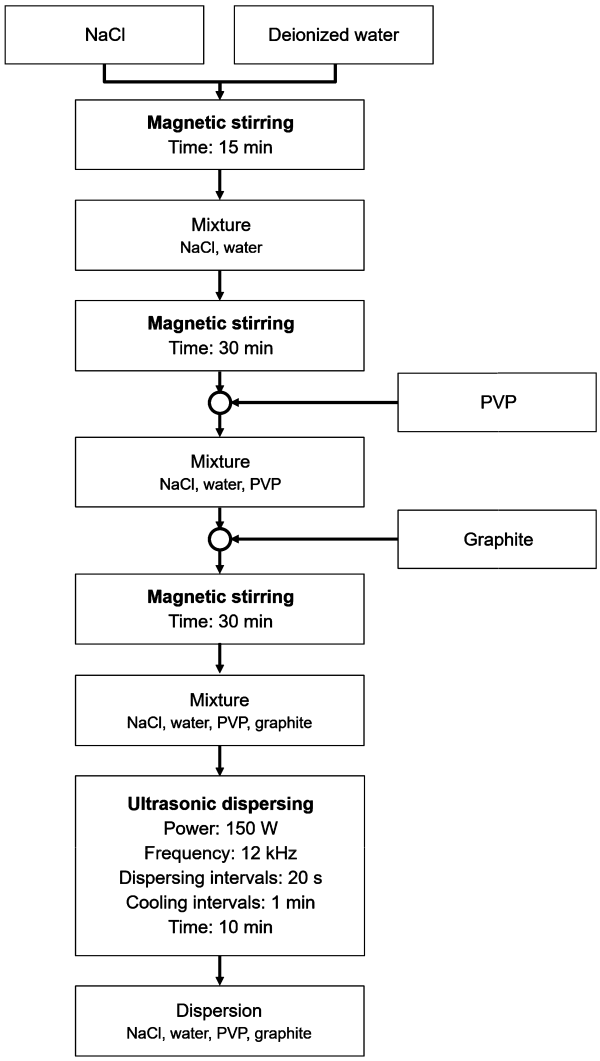

Fig. 5. Process route for the preparation of the dispersions.

The process route applied for the preparation of the dispersions is depicted in Fig. 5. The mixing sequences were carried out at a temperature of 25 °C and ambient pressure. First, the liquid phases were prepared. A 1-molar solution was prepared from the crystalline NaCl, with the concentration adjusted by the mass ratio of salt to water. Subsequently, the dispersant was mixed with the liquid phase and graphite was added. After a stirring period, the dispersions were ultrasonically dispersed using a homogenizer (FS-300N, Vevor, China).

3.2. Experimental procedure

The stability behavior was studied as a function of the PVP content for both derivatives at a constant graphite content of 10 m%. The reliable measurement of the electrophoretic mobility and thus the accurate determination of the zeta potential required the measurement at a defined ionic strength of the samples [53]. However, an increasing ionic strength has a destabilizing effect on the dispersion. To mitigate this influence, the samples were adjusted to the lowest recommended ionic strength of 0.1 mmol/L [53].

3.3. Measuring equipment and methods

Model

The model was calibrated to the *distance of closest approach*, which states that particles cannot approach closer than 0.4 – 0.6 nm [24].

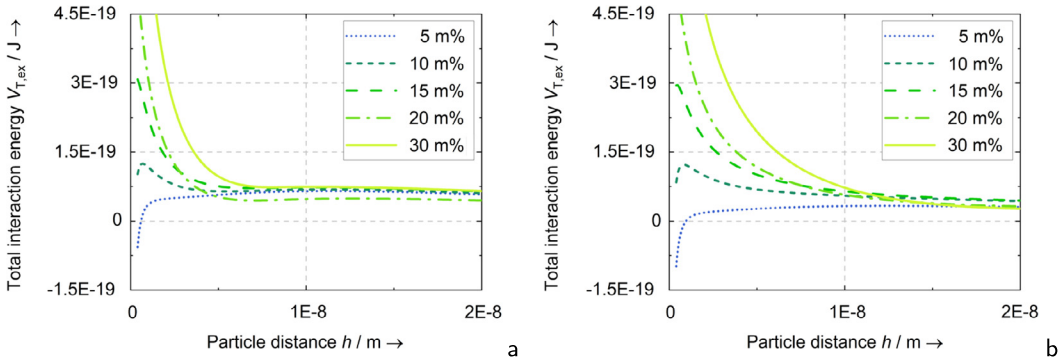

Fig. 6. Total interaction energies $V_{T,ex}$ as a function of the particle distance h for graphite dispersions with a varying PVP content of the PVP derivatives (a) K-17 and (b) K-30.

The complete displacement of the continuous phase would mean that the counterions lose their hydrate shell, which is considered unlikely. This results in a minimum distance from the thickness of two water layers, which corresponds to twice the distance from the particle surface to the outer Helmholtz layer.

The surface potential was approximated by the zeta potential, which represents a common practice in stability studies of low ionic strength dispersions [30]. The zeta potential was calculated by empirically determining the electrophoretic mobility using a zeta potential analyzer (Zetasizer Nano ZSP, Malvern Panalytical, Malvern, UK). Accordingly, the dispersions were diluted to reach the required transmittance of the dispersion. Three measurements were performed for each dispersion.

Since the measured zeta potential is strongly dependent on the pH value of the dispersion, the corresponding pH values of the analyzed dispersions were measured. They are provided in the supplementary files. The pH value was determined using a pH measuring instrument (PH-100 ATC, Voltcraft, Switzerland) with an absolute accuracy of 0.2 pH.

Sedimentation analyses

The dispersions were poured into transparent test cuvettes with a volume of 4 mL. The samples were visually evaluated by a gray scale analysis. The average gray value was determined using the graphics program GIMP. The gray value ranged from 0 (black) to 1 (white) and was normalized to the gray value of the background.

4. Results and discussion

Total interaction energies according to the model

Using the model described in Section 2, the total interaction energies $V_{T,ex}$ (see Equation (27)) were calculated as a function of the particle distance h for K-17 (see Fig. 6a) and K-30 (see Fig. 6b).

It is apparent that for both PVP derivatives, the total interaction energy levels rise with an increasing PVP content in the range of small particle distances. For the dispersions containing 5 m% PVP, no maximum is present. The dispersions with 10 m% PVP show a weakly pronounced maximum. From a PVP content of 15 m% upwards, the energy curves are subject to a major drop, being more distinct with an increasing PVP content.

The relation between the energy curves and the coagulation is described by the stability factor W which is defined as [54]

$$W \approx (a_1 + a_2)^{-1} \cdot \kappa^{-1} e^{\left(\frac{V_{T,ex,max}}{k_B T}\right)}, \tag{28}$$

where $V_{T,ex,max}$ stands for the energy barrier that particles have to overcome to coagulate.

W can be interpreted as the probability of coagulation when two particles collide. It represents the ratio of the total number of collisions to the number of collisions leading to coagulation [24]. The higher $V_{T,ex,max}$ is, the higher is W and thus the less likely is the occurrence of coagulation (see Equation (28)). Accordingly, a maximum of $V_{T,ex}$ represents an energy barrier for the particles, whereas a strong decrease marks an insurmountable barrier [55]. This demonstrates that the graphite dispersions exhibit a pronounced energy barrier for both PVP derivatives above a PVP content of 15 m%. This trend is also reflected in the calculated values $V_{T,ex,max}$ and W (see Fig. 7 and Table 2). Varying statements can be found regarding the categorization of the dispersions into *stable* and *non-stable* using these characteristic values. According to Verwey and Overbeek [24], a stable dispersion can be expected for a stability factor $W \geq 10^5$. To ensure stability for all practical purposes, the stability factor W is required to exceed $1 \cdot 10^9$. Here, it should be noted that the conditions for the practical purposes are not further defined. According to this rule of thumb, stability can be expected for the dispersions containing at least 10 m% for both derivatives. However, the sedimentation analyses showed that stability is only given for dispersions with a minimum of 15 m% PVP.

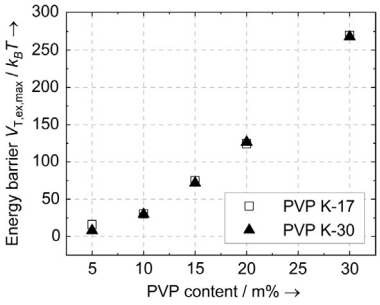

Fig. 7. Calculated values for $V_{T,ex,max}$ as a function of the PVP content.

Table 2. Calculated values for $V_{T,ex,max}$ and W of the graphite dispersions at different PVP contents for the PVP derivatives K-17 and K-30.

		$V_{T,ex,max}$ in $k_B T$	W
5 m% PVP	K-17	15.88	$6.2 \cdot 10^6$
	K-30	8.01	$1.7 \cdot 10^3$
10 m% PVP	K-17	30.31	$1.1 \cdot 10^{13}$
	K-30	29.78	$4.9 \cdot 10^{12}$
15 m% PVP	K-17	74.81	$2.4 \cdot 10^{32}$
	K-30	71.7	$7.8 \cdot 10^{30}$
20 m% PVP	K-17	124.31	$7.6 \cdot 10^{53}$
	K-30	126.49	$4.9 \cdot 10^{54}$
30 m% PVP	K-17	269.65	$1.0 \cdot 10^{117}$
	K-30	267.81	$1.2 \cdot 10^{116}$

Sedimentation analyses

Fig. 8 displays the average gray value over time for graphite dispersions with a varying PVP content of K-17 (see Fig. 8a) and K-30 (see Fig. 8b).

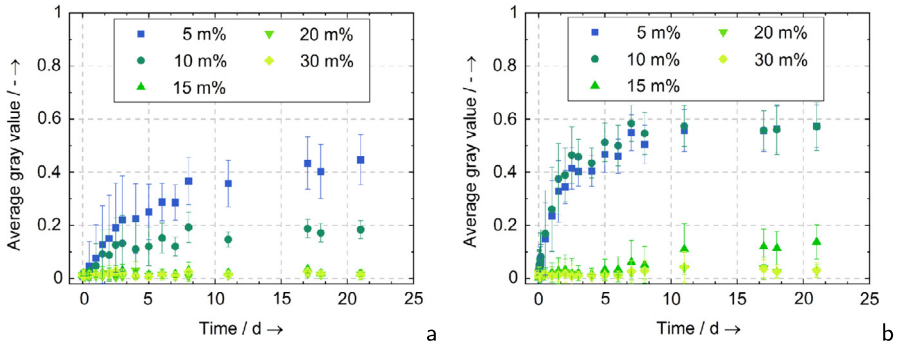

Fig. 8. Average gray value as a function of the time for graphite dispersions with a varying PVP content of the PVP derivatives (a) K-17 and (b) K-30.

Overall, it is apparent that the gray values of the graphite dispersions with K-17 are lower than with K-30 at the same PVP content. Furthermore, it is evident that the lower the PVP content is, the higher is the increase in the gray values.

For both PVP derivatives, the dispersions with 5 m% and 10 m% PVP, respectively, show a significant increase in the gray values within the first few days. This effect is more pronounced for the dispersions with 10 m% PVP than for the ones with 5 m% PVP. While the average gray value of the dispersions with 15 m% PVP remains almost constant over the investigated time duration for K-17, a minor increase in the gray value can be observed for K-30 after four days. For both K-17 and K-30, the dispersions containing 20 m% and 30 m% PVP, respectively, remain almost stable over the investigated duration.

A constant gray value indicates a stable dispersion without considerable coagulation, whereas an increase in the gray value implies the occurrence of coagulation. These observations can be explained by the prevailing phenomena on the particle level. The behavior of particles in the nanometer range is dominated by Brownian forces [56]. As a result, the particles do not settle due to gravity. A reversible equilibrium structure is established, which prevents the particles from sinking [56]. When the particles coagulate, Brownian motion no longer appears. The sedimentation behavior due to gravity dominates the motion of the particles, which can be mathematically described by the Stokes' law [57]. For a spherical particle, this results in the following equation for the flow velocity v [12, 56]:

$$v = \frac{2}{9}\frac{(\rho_p - \rho_s)}{\eta} \cdot g \cdot r^2. \tag{29}$$

Here, ρ_p and ρ_s are the densities of the particles and the medium. g is the gravitational field strength, η the viscosity, and r the particle radius.

It follows from Equation (29) that the particle radius has a quadratic influence on the flow velocity and thus on the sedimentation time. Low PVP contents are not sufficient to significantly weaken the attractive forces between the particles and thus are not capable of preventing coagulation [41]. As a result, the coagulated particle formations settle more quickly. At higher PVP contents, the graphite particle surfaces are increasingly occupied by PVP molecules, which successively inhibits the attractive forces due to electrosteric stabilization [41].

Comparison of the data

When comparing the calculated energy levels with the gray value data in terms of the PVP content, it is obvious that the trend of the energy levels corresponds well with the trend of the gray value curves. While the energy levels exhibit higher values with an increasing PVP content, the gray value curves show an ever smaller increase.

A slight deviation can be recognized in the evaluation of the stability based on the stability factor W. While the dispersions with 10 m% appear to be unstable according to the gray value progression, the stability factor W is higher than the stability threshold of $1 \cdot 10^9$ for practical purposes. This indicates that this limit defined by Verwey and Overbeek [24] may slightly deviate depending on the practical application. Accordingly, the limit value has not yet been subjected to an application-related and thus time-dependent scale. For the other dispersion compositions, the behavior observed in the sedimentation analyses agrees very well with the classification given by the stability factor W.

Overall, the findings corroborate the assumption of Yangshuai et al. [15] that a modeling approach based on the extended DLVO theory is suitable to reproduce the stability behavior of aqueous graphite dispersions. In addition, the results demonstrate that it is feasible to incorporate the effects originating from an electrosteric polymer into the DLVO theory.

5. Conclusions

This paper presents an analytical modeling approach to describe the stability of water-based graphite dispersions containing the electrostatically stabilizing dispersant PVP on the basis of the extended DLVO theory. Two different PVP derivatives, K-17 and K-30, were studied. The model was adapted to capture the boundary conditions that apply to the investigated dispersion system. The total interaction energies were calculated using empirical data obtained from zeta potential measurements. The stability behavior was examined by sedimentation analyses. The findings of this paper can be summarized as follows:

- The model elaborated on the basis of the extended DLVO theory is applicable to aqueous graphite dispersions.
- The incorporation of the dispersant polyvinylpyrrolidone and the associated effects in the model has proven to be feasible.
- The sedimentation analyses showed that the trend of the obtained gray value data can be represented very well by the calculation of the total interaction energy levels. Therefore, the results corroborate that the elaborated model is well suited to describe the stability behavior of water-based graphite dispersions containing PVP.

Further research will be conducted to derive absolute values for the stability factor W, which allows a time-dependent evaluation of the dispersion stability depending on the particular application.

Due to the universality of the developed model, it is expected to be transferable to different material and dispersant systems. Additional effort is required to prove the transferability on a profound basis. In this context, the applicability of the model to water-based graphene dispersions remains to be validated.

Declarations

Author contribution statement

Cara Greta Kolb: Conceived and designed the experiments; Performed the experiments; Analyzed and interpreted the data; Contributed reagents, materials, analysis tools or data; Wrote the paper.

Maja Lehmann: Analyzed and interpreted the data.

Dominik Kulmer: Conceived and designed the experiments; Performed the experiments; Analyzed and interpreted the data.

Michael Friedrich Zaeh: Analyzed and interpreted the data; Contributed reagents, materials, analysis tools or data.

Funding statement

Ms. Cara Greta Kolb was supported by Federal Ministry of Education and Research (BMBF) [ExZellTUM III, 03XPO255].

Data availability statement

Data included in article/supp. material/referenced in article.

Declaration of interests statement

The authors declare no conflict of interest.

Additional information

Supplementary content related to this article has been published online at https://doi.org/10.1016/j.heliyon.2022.e11988.

References

[1] K. Pan, Y. Fan, T. Leng, J. Li, Z. Xin, J. Zhang, L. Hao, J. Gallop, K. Novoselov, Z. Hu, Sustainable production of highly conductive multilayer graphene ink for wireless connectivity and IoT applications, Nat. Commun. 9 (2018) 1–10.
[2] U. Kamran, Y. Heo, J. Lee, S. Park, Functionalized carbon materials for electronic devices: a review, Micromachines 10 (2019) 234.
[3] Y. Lin, D. Gritsenko, Q. Liu, X. Lu, J. Xu, Recent advancements in functionalized paper-based electronics, ACS Appl. Mater. Interfaces 8 (2016) 501–20 515.
[4] D. Andre, H. Hain, P. Lamp, F. Maglia, B. Stiaszny, Future high-energy density anode materials from an automotive application perspective, J. Mater. Chem. A 5 (2017) 174–17 198.
[5] S. Lanceros-Méndez, C. Costa, Printed Batteries: Materials, Technologies and Applications, John Wiley & Sons, Hoboken, 2018.
[6] M. Ervin, L. Le, W. Lee, Inkjet-printed flexible graphene-based supercapacitor, Electrochim. Acta 147 (2014) 610–616.
[7] S. Delekta, A. Smith, J. Li, M. Oestling, Inkjet printed highly transparent and flexible graphene micro-supercapacitors, Nanoscale 9 (2017) 6998–7005.
[8] C.G. Kolb, M. Lehmann, J. Kriegler, J.-L. Lindemann, A. Bachmann, M. Zaeh, Qualifying water-based electrode dispersions for the inkjet printing process: a requirements analysis, Rapid Prototyping J. 28 (2022).
[9] P. Delannoy, B. Riou, T. Brousse, J. Le Bideau, D. Guyomard, B. Lestriez, Ink-jet printed porous composite $LiFePO_4$ electrode from aqueous suspension for microbatteries, J. Power Sources 287 (2015) 261–268.
[10] S. Hoath, Fundamentals of Inkjet Printing: the Science of Inkjet and Droplets, John Wiley & Sons, Hoboken, 2016.
[11] H. Wijshoff, The dynamics of the piezo inkjet printhead operation, Phys. Rep. 491 (2010) 77–177.
[12] D. Genovese, Shear rheology of hard-sphere, dispersed, and aggregated suspensions, and filler-matrix composites, Adv. Colloid Interface Sci. 171 (2012) 1–16.
[13] B. Derby, N. Reis, Inkjet printing of highly particulate suspensions, Mater. Res. Soc. Bull. 28 (2003) 815–818.
[14] Y. Guo, H. Patanwala, B. Bognet, A. Ma, Inkjet and inkjet-based 3D printing: connecting fluid properties and printing performance, Rapid Prototyping J. 23 (2017) 562–576.
[15] Q. Yangshuai, Y. Yongfu, Z. Lingyan, P. Weijun, Q. Yupeng, Dispersion and agglomeration mechanism of flaky graphite particles in aqueous solution, J. Dispers. Sci. Technol. 38 (2017) 796–800.
[16] Y. Chen, L. Zhou, J. Wei, C. Mei, S. Jiang, M. Pan, C. Xu, Direct ink writing of flexible electronics on paper substrate with graphene/polypyrrole/carbon black ink, J. Electron. Mater. 48 (2019) 3157–3168.
[17] T. Tadros, Rheology of Dispersions: Principles and Applications, John Wiley & Sons, Hoboken, 2011.
[18] C. Kolb, M. Lehmann, J. Lindemann, A. Bachmann, M. Zaeh, Improving the dispersion behavior of organic components in water-based electrode dispersions for inkjet printing processes, Appl. Sci. 11 (2021) 2242.
[19] M. Lehmann, C. Kolb, F. Klinger, M. Zaeh, Preparation, characterization, and monitoring of an aqueous graphite ink for use in binder jetting, Mater. Des. 207 (2021) 109871.
[20] B. Utela, D. Storti, R. Anderson, M. Ganter, Development process for custom three-dimensional printing 3DP material systems, J. Manuf. Sci. Eng. 132 (2010) 011008.
[21] Y. Htwe, M. Mariatti, Surfactant-assisted water-based graphene conductive inks for flexible electronic applications, J. Taiwan Inst. Chem. Eng. 125 (2021) 402–412.
[22] W. Russel, D. Saville, W. Schowalter, Colloidal Dispersions, Cambridge University Press, Cambridge, 1991.
[23] B. Derjaguin, L. Landau, Theory of the stability of strongly charged lyophobic sols and of the adhesion of strongly charged particles in solutions of electrolytes, Acta Physicochim. USSR 14 (1941) 30–59.
[24] E. Verwey, J. Overbeek, Theory of the stability of lyophobic colloids, J. Phys. Chem. 51 (1947) 631–636.
[25] T. Mitchell, A. Nguyen, G. Evans, Heterocoagulation of chalcopyrite and pyrite minerals in flotation separation, Adv. Colloid Interface Sci. 114 (2005) 227–237.
[26] A. Nguyen, H.J. Schulze, Colloidal Science of Flotation, Taylor & Francis Inc, London, 2003.
[27] L. Liu, M. Gonzalze-Olivares, H. Bai, H. Yi, S. Song, Colloidal stability of silica and graphite in aqueous suspensions, Chem. Phys. 525 (2019) 110405.
[28] T. Wakamatsu, Y. Numata, Flotation of graphite, Miner. Eng. 4 (1991) 975–982.
[29] M.M. Gudarzi, Colloidal stability of graphene oxide: aggregation in two dimensions, Langmuir 32 (2016) 5058–5068.
[30] R. Yoon, D. Flinn, Y. Rabinovich, Hydrophobic interactions between dissimilar surfaces, J. Colloid Interface Sci. 185 (1997) 363–370.
[31] M. Zhu, J. Park, A. Sastry, Particle interaction and aggregation in cathode material of Li-ion batteries: a numerical study, J. Electrochem. Soc. (2011) A1155.
[32] J. Seebergh, J. Berg, Depletion flocculation of aqueous, electrosterically-stabilized latex dispersions, Langmuir 10 (1994) 454–463.
[33] S. Kumar, D. Ray, S. Abbas, D. Saha, V. Aswal, J. Kohlbrecher, Reentrant phase behavior of nanoparticle solutions probed by small-angle scattering, Curr. Opin. Colloid Interface Sci. 42 (2019) 17–32.
[34] J. Zhang, H. Zeng, Intermolecular and surface interactions in engineering processes, Engineering 7 (2021) 63–83.
[35] R. Pashley, Attractive forces between uncharged hydrophobic surfaces: direct measurements in aqueous solution, Science 229 (1985) 1088–1089.
[36] J. Israelachvili, Adhesion forces between surfaces in liquids and condensable vapours, Surf. Sci. Rep. 14 (1992) 109–159.
[37] H. Hamaker, The London-van der Waals attraction between spherical particles, Physica 4 (1937) 1058–1072.
[38] D. Prieve, W. Russel, Simplified predictions of Hamaker constants from Lifshitz theory, J. Colloid Interface Sci. (1988) 1–13.
[39] A. Anandarajah, J. Chen, Single correction function for computing retarded van der Waals attraction, J. Colloid Interface Sci. (1995) 293–300.
[40] B. Pailthorpe, W. Russel, The retarded van der Waals interaction between spheres, J. Colloid Interface Sci. 89 (1982) 563–566.
[41] S. van Guyen, D. Rouxel, R. Hadji, B. Vincent, Y. Fort, Effect of ultrasonication and dispersion stability on the cluster size of alumina nanosclae particles in aqueous solutions, Ultrason. Sonochem. 18 (2011) 382–388.
[42] J. Israelachvili, Intermolecular and Surface Forces, Elsevier, Waltham, 2011.
[43] C. Likos, K. Vaynberg, H. Loewen, N. Wagner, Colloidal stabilization by adsorbed gelatin, Langmuir 16 (2000) 4100–4108.
[44] Y. Kamiyama, J. Israelachvili, Effect of ph and salt on the adsorption and interactions of an amphoteric polyelectrolyte, Macromolecules 25 (1992) 5081–5088.
[45] V. Bühler, Polyvinylpyrrolidone Excipients for Pharmaceuticals: Povidone, Crospovidone and Copovidone, Springer Science & Business Media, Berlin, 2005.
[46] X. Sui, Y. Chu, J. Zhang, H. Zhang, H. Wang, T. Liu, C. Han, The effect of pvp molecular weight on dissolution behavior and physicochemical characterization of glycyrrhetinic acid solid dispersions, Adv. Polym. Technol. (2020).
[47] J. Li, K. Inukai, Y. Takahashi, A. Tsuruta, W. Shin, Effect of PVP on the synthesis of high-dispersion core-shell barium-titanate-polyvinylpyrrolidone nanoparticles, J. Asian Ceram. Soc. 5 (2017) 216–225.
[48] N. N. Technology, High Purity Natural Graphite: Nanopowder/Nanoparticles for Li-Ion Battery, Nanografi Nano Technology, Ankara, 2021.
[49] G. Lauth, J. Kowalczyk, Einführung in die Physik und Chemie der Grenzflächen und Kolloide, Springer, Heidelberg, 2016.
[50] B. Vincent, J. Edwards, S. Emmett, A. Jones, Depletion flocculation in dispersions of sterically-stabilised particles ("soft spheres"), Colloids Surf. 18 (1986) 261–281.
[51] A. Jones, B. Vincent, Depletion flocculation in dispersions of sterically-stabilised particles 2. Modifications to theory and further studies, Colloids Surf. 42 (1989) 113–138.
[52] A.H. Pelofsky, Surface tension-viscosity relation for liquids, J. Chem. Eng. Data 11 (1966) 394–397.
[53] G. Lowry, R. Hill, S. Harper, A. Rawle, C. Hendren, F. Klaessig, U. Nobbmann, P. Sayre, J. Rumble, Guidance to improve the scientific value of zeta-potential measurements in nanoehs, Environ. Sci. Nano 3 (2016) 953–965.
[54] Q. Wang, On colloidal suspension Brownian stability ratios: theoretical approaches, J. Colloid Interface Sci. 145 (1991) 99–107.
[55] A. Kulshreshtha, O. Singh, G. Wall, Pharmaceutical Suspensions: from Formulation Development to Manufacturing, Springer Science & Business Media, Berlin, 2009.
[56] J. Mewis, Flow behavior of concentrated suspensions: predictions and measurements, Int. J. Miner. Process. 44 (1996) 17–27.
[57] S. Ramaywamy, Issues in the statistical mechanics of steady sedimentation, Adv. Phys. 50 (2001) 297–341.